Hindawi
Mobile Information Systems
Volume 2022, Article ID 9523208, 10 pages
https://doi.org/10.1155/2022/9523208

Research Article

Key Technology of Wide-Area Backup Protection of Intelligent DC Power Networks Based on Fault Identification

Chongyu Cui,[1] **Zhaoxia Li**,[1] **Hongmei Wu**,[1] **and Xiaojia Sun**[2]

[1]*College of Electrical Engineering, Tibet Agricultural and Animal Husbandry University, Nyingchi 860000, Tibet, China*
[2]*State Grid Tibet Electric Power Research Institute, Lhasa 850000, Tibet, China*

Correspondence should be addressed to Chongyu Cui; cuichongyu@xza.edu.cn

Received 10 May 2022; Revised 13 July 2022; Accepted 27 July 2022; Published 23 August 2022

Academic Editor: Abid Yahya

As the size of the grid continues to grow, traditional backup protection is no longer sufficient to meet the needs of the grid in complex environments. The key to wide-area protection is the concept of making full use of the wide-area information measured in the grid to identify faults. This paper first describes the architecture of a wide-area defense team and then proposes a fault line detection algorithm based on normal fault assembly wide-area backup protection and a positive matrix based on spectral analysis. In the assembly-based positive sequence error discovery algorithm, the difference in the amount of fault judgment between line zone faults and out-of-zone faults is illustrated, and fault line detection criteria are given. In the algorithm based on random matrix spectrum analysis, the current error sequence of each pin of the circuit is copied, translated, and superimposed with noise, then the original random matrix is matrix transformed according to random matrix theory to obtain the fault identification matrix, and finally the average spectrum radius is calculated. Through the simulation of the IEEE10 machine 39-node standard test model, it is proved that the two algorithmic methods proposed in our article can accurately identify faulty lines under various fault conditions.

1. Introduction

China's economy is developing rapidly, which has led to an increasingly large and complex power grid [1]. While grid interconnections bring optimistic economic benefits to industrial production, they also bring a range of problems that cannot be ignored. Unlike small and medium-sized grids, the losses caused by large-scale interconnected grids can be severe [2]. In addition, the probability of accidents is high under the influence of factors such as the deterioration of the natural environment [3]. In 2017, an electricity tower in Hualien, Taiwan, was blown down by a typhoon. Taiwan was plunged into a "power outage crisis" that lasted for nearly a week, causing massive power outages and affecting 6.88 million households, not including all kinds of factories and enterprises. In the face of such huge economic losses, the security of the electricity network is gradually drawing attention. In the event of a failure, we want to be able to identify and isolate fault areas quickly and accurately to ensure safe and reliable network performance [4, 5]. Therefore, it is necessary to study the wide-area backup protection technology of power grid in order to reduce the economic loss and security risk caused by power failure.

In order to cope with the development of power grids and to solve the problems of existing wide-area protection systems, experts and scholars have now started to focus on this area. In the area of wide-area protection, foreign research started earlier. in 1997, the Swedish scholar Ingelsson et al. [6] pioneered the concept of wide-area protection for grid security. He established a SCADA-based wide-area protection system to realize safety automatic control functions and pointed out that the system was mainly used to prevent voltage collapse in case of serious faults. Then in 1998, the Japanese scholar Serizawa et al. [7] proposed the use of network-wide information to realize galvanic protection and backup protection for a wide range of current differences. This was the first time that the concept of wide-area protection was introduced to relay protection, emphasizing the use of wide-area information to improve the performance of the support system. Mallikarjuna et al. [8]

proposed a multiphase measurement unit (MPMU) based on the ASWABP scheme to improve the safety and stability of the power system. This approach allows monitoring of standby security using a wide range as in conventional range security. Mirhosseini and Akhbari [9] introduced a novel wide-area reserve coverage algorithm based on complex power of faulty elements to solve the problems in conventional support systems and eliminate the high-stress power supply chain operation requirements. Domestic research on wide-area reserve protection started late, but inspired by foreign research results, many experts and scholars have started to research on wide-area reserve protection for power grid. Jia et al. [10] considered the problem of alternative paths after the main path link or node failure and proposed a multi-path routing algorithm based on ant colony algorithm to improve the reliability of wide-area protection communication. Shan et al. [11] proposed a new algorithm for identifying bus faults in wide-area protection support to improve the accuracy and error resistance of wide-area support coverage. The method combines the collected line direction information with protection information to obtain a comprehensive value for busbar protection. Liu et al. [12] introduced a new gray correlation analysis and multi-information fusion of sequence currents for a wide-area protection-based backup strategy. The wide-area fault resistance to support safety is further improved, and the fault location can be accurately identified even under complex conditions. Song et al. [13] determine the fault location by fault tolerance based on the fault distance I and II information and error direction signals within the protection range. Therefore, an IED-based highly fault-tolerant wide-area standby protection algorithm is proposed for distributed wide-area standby protection systems between substations. He et al. [14] introduced protection for wide-area support zoning problem, combined with map theory search path data, using fuzzy comprehensive evaluation method to determine the central station location and then search for a convenient area for zoning. Tong et al. [15] were more sensitive to the transition resistance of the wide-area backup protection algorithm. The wide-area active power (DAP) is proposed under the phasor measurement unit (PMU). The power security of urban rail transit power supply system is very important. Wei and Changet al. [16] proposed a wide-area fallback scheme with large coverage of state information for the traditional relay protection of urban rail transit power supply systems. The scheme adaptively adjusts protection measures through relay protection information sharing. Wang et al. [17] proposed a wide-area fallback protection fault discrimination algorithm using multi-point voltage estimation to achieve fast and accurate identification of faulty lines under limited PMU. The method solves for the fault point location based on the voltage estimation. In summary, experts and scholars at home and abroad have achieved fruitful results in the field of wide-area backup protection, effectively promoting the further development of wide-area backup protection research.

Although experts and scholars at home and abroad have proposed many methods for wide-area standby identification, the following shortcomings still exist due to the huge and complex nature of power networks. Firstly, after a fault occurs in the power system, it is difficult for the existing methods to locate the fault area accurately. The rapid and accurate location of faults facilitates power restoration and helps to reduce economic losses. Secondly, wide-area backup protection is a supplement and backup to the main protection, and today's distribution network data are huge. This places higher demands on the identification of faulty lines for wide-area backup protection, and valuable information must be extracted from the vast amount of data. Finally, the existing backup protection methods are computationally intensive, difficult to implement, and fault-tolerant to be further improved.

Once a fault has occurred on a grid line, the location of the fault needs to be determined. Fault identification algorithms require a large amount of information and involve many electrical components. Missing or erroneous measurement information is inevitable during the transmission of information. Wide-area backup protection that relies solely on a single source of information can hardly fulfil fault identification requirements in the event of poor or incorrect information [18]. At present, in the field of wide-area backup protection, the research on fault identification algorithms mainly focuses on using wide-area redundant information to improve the accuracy of fault identification. That is, in the case of missing or wrong information, reasonable use of electrical quantity and switch quantity and its fusion information can improve fault tolerance of backup protection. Wang [19] applied the fault identification method to a mining conveyor belt and effectively solved the problem of vertical tear image detection and vertical tear fault identification for mining conveyor belts. Wang et al. [20] detected serial DC arc faults and effectively reduced the threat to DC power systems. Zhu et al. [21] identified and classified fault samples in process industries, reducing the errors caused by unbalanced sample sets. Jia et al. [22] applied fault identification methods to the study of faults in high-speed trains, which enabled high-speed trains to return to normal operation quickly and accurately. Ma et al. [23] used a fault identification method based on parameter optimization to diagnose the bearings of packaging machinery power machines and improve their reliability. Chen [24] identified faults in transmission lines, reducing the hidden danger of line faults, ensuring the safe and stable operation of the transmission and distribution network, and better meeting the public's demand for electricity. Li et al. [25] carried out fault detection for fan blade cracks, providing a basis and means for normal blade, abnormal condition detection, and crack length status. From the above, it can be seen that through fault identification, problems can be effectively detected, which helps to restore the normal operation status of the equipment quickly and effectively. Therefore, this paper considers the key technology to study the wide-area backup protection of intelligent DC power networks based on fault identification.

A fault line detection method using a normal serial error component and a wide-area random array-based backup protection method are proposed to address the high latency

and complex timing problems of conventional backup protection actions. In a fault line detection fault assembly-driven system based on the fault line detection, the difference between the amount of line area faults and out-of-area faults judged is explained and fault line detection criteria are given for the fault attached network when a line fault occurs. In the random matrix spectrum analysis based on the wide-area protection backup alarm technique, the average wide-area optical field radius line is calculated by generating a fault identification matrix. The average optical frequency diameter value calculated from the measured data is compared with a threshold value to identify the faulty line. Through simulation experiments on the IEEE10 machine 39-node standard test model, it is demonstrated that the proposed scheme is able to accurately identify faulty lines under various fault conditions.

2. Methods

2.1. Wide-Area Protection System Architecture. According to the voltage level of the power system, the protection object, and the communication technology, combined with the requirements of the protection action time, the wide-area protection system is generally divided into substation distributed system, regional distributed protection system, and hierarchical control system.

(1) Substation distributed system. It can be divided into three layers: station control layer, compartment layer, and process layer. Each layer is composed of different equipment or subsystems to complete corresponding functions. In this system, each substation has a protection host that implements station domain protection. The main source of information for the protection host is the station domain information uploaded by the station protection/control devices; the secondary protection information source comes from the interaction between the station domain host and the station host at other substations. The station domain protection mainframe integrates these two sources of information, detects fault point information between stations, and optimizes the station domain protection. This level of system is suitable for station main protection or station domain standby protection.

(2) Regionally distributed protection system. In this system, several substations form a zone according to the zoning principle and one substation is designated as the protection center for the zone. The substation distributed system is a special case of a regionally distributed protection system. The system can be divided into two parts. The first part is the station domain protection host receiving and preprocessing real-time information uploaded by the protection/control unit or PMU and uploading the processed information to the regional protection center. At the same time, the mainframe in the station domain can receive control and dispatch from the regional dispatch center. The other part is the regional protection center, which collects load factor, fault information, and breaker opening and closing status information from the substations in the region to form a wide-area dynamic information network for fault location or wide-area status estimation. This center is responsible for tasks such as backup protection or system operation optimization in the region. Based on the above analysis, a regionally distributed protection system applying the new power electronics will be very suitable for optimizing inter-station load rates, regional state estimation, and station backup protection.

(3) A hierarchical protection and control system. The architecture is based on a regionally distributed protection system and a substation centralized one and covers the entire large area of the grid. The architecture system of the hierarchical protection and control system is divided into two parts: the substation distributed system (intelligent substation) and the regionally distributed protection system. The station host of the substation distributed system is connected to the process layer communication network of the station, and the PMU or merging unit in the integrated station collects the information of the whole station, realizes data processing, and sends protection control commands. The regionally distributed protection system extends substation functions to regional master stations in each region, which interact with each other for information and realize regional protection functions.

2.2. Faulty Line Detection Algorithm Based on Positive Sequence Fault Components

2.2.1. Principle of Line Fault Detection Based on Positive Sequence Fault Elements. When a fault occurs on a line, the positive sequence fault component exists in a variety of fault situations. The positive sequence fault component is studied as an example in our article. Positive sequence fault component is not affected by the system power potential; positive sequence fault components exist under different fault types; the positive sequence fault component voltage is the largest at the fault point. According to the superposition principle, the fault state of the line is decomposed into a prefault state (load state) and a fault connection state. The positive sequence current fault component is a sudden change $\Delta I_i = I_i - I_{i-nN}$, which reflects the fault state of the line, irrespective of the losses through the load flow and the bridge impedance. The main protection action rate is typically no more than 30 ms, and the fault component typically lasts 40 ms ($n = 2$), which is sufficient to allow the main protection criterion to identify the fault. When n is taken as 2, the positive sequence current fault component tends to zero in the steady-state phase after the transient state and exists for a short period of time, which is not conducive to utilizing the steady-state volume of the fault component after a two-cycle fault. The fault component used in this paper refers to the six precycle current signals subtracted

from the current signal. The fault component can reflect the characteristics of the transient phase and the steady-state phase of the last 6 cycles after a line fault has occurred.

Let line ij be an Earth fault at end a of bus i. The fault-added network in the event of a fault on the line is shown in Figure 1. Each current and voltage variable in the figure is a positive sequence fault component. ΔI_i, ΔI_j, ΔV_i, ΔV_j for bus i, j at the current and voltage fault components, respectively, R_f for the transition resistance, ΔI_f for the current fault component flowing through the fault branch, ΔU_f for the fault point F at the potential, Z for the line ij positive sequence impedance, and Z_i and Z_j for bus i, j on both sides of the system equivalent impedance, respectively.

When an Earth fault occurs online ij,$_f$, a potential fault component appears at the short-circuit point F of the additional network ΔU_f and the fault current flowing through the transition resistor $R\Delta I_f$, which can be derived from the basic circuit principle.

$$\Delta \dot{I}_f = \frac{\Delta \dot{U}_f}{\left(R_f + (aZ + Z_i) \cdot \left((1-a)Z + Z_j\right)/Z_i + Z_j + Z\right)}. \tag{1}$$

According to Kirchhoff's current law, we can know the fault components of the currents flowing through buses i and $j\Delta I_i$ and ΔI_j and obtain the fault component judgment quantity d for this paper, which is a real number greater than 1.

$$d = \frac{\left|\Delta \dot{I}_i + \Delta \dot{I}_j\right|}{\left|\Delta \dot{I}_i - \Delta \dot{I}_j\right|} = \frac{\left|Z_i + Z_j + Z\right|}{\left|Z_j + Z - Z_i - 2aZ\right|}. \tag{2}$$

As can be seen from the above equation, d is only related to the impedance of the line, the equivalent impedance of the system on the backside of the two ends and the fault location, and not to the transition resistance, which means that there is no effect of migration resistance on this method in the results of the theoretical analysis.

When an out-of-area fault occurs, the network to which the fault is connected is shown in Figure 2.

The fault additional electromotive force is outside bus j. The current fault components at bus i and $j\Delta I_i$ and ΔI_j are calculated via ΔU_f

$$\Delta \dot{I}_j = -\Delta \dot{I}_i = \frac{\Delta \dot{U}_f \cdot Z_j}{R_f \cdot \left(Z_i + Z_j + Z + Z_O\right) + Z_j\left(Z_i + Z_O + Z\right)}. \tag{3}$$

From the above formula, flowing through the bus i, j of the current fault component phase opposite, the amplitude is basically the same. At this point, the normal line d value is much less than 1, approximately equal to 0.

$$d = \frac{\left|\Delta \dot{I}_i + \Delta \dot{I}_j\right|}{\left|\Delta \dot{I}_i - \Delta \dot{I}_j\right|} \approx 0 \ll 1. \tag{4}$$

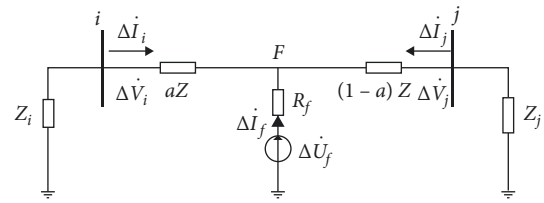

Figure 1: Faulty connection network in the region.

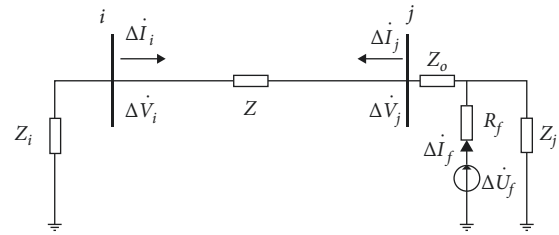

Figure 2: Faulty component add-on network for out-of-zone faults.

In summary, the d values corresponding to faults in the area and faults outside the area are very different. When the fault occurs within the area, the line has a d greater than 1, whereas when the fault occurs outside the area, the fault d is greater than 1. Therefore, the faulty line can be identified by comparing the d value with a given threshold value, which is set to 1.

2.2.2. Fault Line Detection Criteria Based on Current Fault Components

(1) When a line L_i has a protective element actuated, d_i is calculated for the line L_i. When three consecutive d_i are greater than 1, L_i is identified as a faulty line; i.e., the fault detection criterion 1 based on the current fault component is

$$\left(d_i(t-2) > 1\right) \cap \left(d_i(t-1) > 1\right) \cap \left(d_i(t) > 1\right) = 1, \tag{5}$$

where d_i (t) represents the d_i calculated from the current fault component at the current time and d_i $(t-1)$ represents the d_i calculated from the current fault component at the previous moment.

(2) When the continuous d of line L_{ii} is less than 1, the distance protection oscillation blocking element is detected if it is activated. If activated, the fault position value a of line L_{ii} is resolved by the fault element. If there are three consecutive $a_i \epsilon$ (0,1), then line L_i is considered to be a faulty line, i.e., detection criterion 2.

$$\begin{cases} \text{Distance.protection.oscillation.blocking.element.starts} \\ a_i \in (0,1) \end{cases} \tag{6}$$

The two criteria above also apply to the calculation of negative and zero sequence currents.

2.3. Wide-Area Backup Protection Algorithm Based on Random Matrix Spectrum Analysis

2.3.1. Fault Line Identification Algorithm Based on Random Matrix Spectrum Analysis. The concept of random matrix theory was first introduced in mathematical statistics by Wishart and Hsu in 1928. The random matrix theory obtains the empirical spectrum distribution of the internal state quantity through the statistical analysis of the energy spectrum and characteristic state of the data matrix, and describes the fluctuation characteristics of the data through the empirical spectrum distribution. According to most of the literature, the mean spectral radius is used as an indicator for data correlation analysis, while the random matrix is analyzed by means of the single-loop theorem.

(1) Generation of Fault Identification Matrix. It means that for each fault, the membership degree of each fault cause can be obtained by multiplying the collected symptom component value and the diagnosis matrix coefficient.

The sequence of fault fractions of the electrical flow at the two ends of the circuit takes the following form.

$$I_{\text{original}} = \begin{bmatrix} \Delta i_1(k_1) & \Delta i_1(k_2) & \cdots & \Delta i_1(k_n) \\ -\Delta i_2(k_1) & -\Delta i_2(k_2) & \cdots & -\Delta i_2(k_n) \end{bmatrix}_{2\times n}, \tag{7}$$

$\Delta i_1(k)$ and $-\Delta i_2(k)$ are the sampled values of the current fault components at both ends of the line, and $k_1, k_2, \ldots, k_n$ is the sampling time. Ioriginal is a $2 \times n$ matrix.

Ioriginal is copied $m-1$ times in a row and expanded after translation to a $2m \times n$ matrix Icopy.

$$I_{copy} = \begin{bmatrix} \Delta i_1(k_1) & \Delta i_1(k_2) & \ldots & \Delta i_1(k_n) \\ -\Delta i_2(k_1) & -\Delta i_2(k_2) & \ldots & -\Delta i_2(k_n) \\ & \vdots \quad \vdots \quad \vdots & & \\ & \vdots \quad \vdots \quad \vdots & & \\ \Delta i_1(k_1) & \Delta i_1(k_2) & \ldots & \Delta i_1(k_n) \\ -\Delta i_2(k_1) & -\Delta i_2(k_2) & \ldots & -\Delta i_2(k_n) \end{bmatrix}_{2m\times n}. \tag{8}$$

A Gaussian white noise matrix of $2m \times n$ is superimposed on the newly formed matrix I_{copy} so that the data in each row and column are not identical and the correlation of the data is reduced. The matrix after superimposing Gaussian white noise is I_{or}.

$$I_{\text{or}} = I_{\text{copy}} + A * N_{\text{gas}}, \tag{9}$$

where $N_{\text{gas}} \in R^{2m\times n}$ is the noise matrix, the elements of N_{gas} are random numbers that follow a standard normal distribution, the letter A is the amplitude of the noise, and I_{or} is the original random matrix of this paper.

Influenced by the line distribution capacitance, when the fault occurs, the current fault component waveforms at both ends of the normal line do not completely coincide. So, the algorithm chooses the superimposed noise amplitude to be half the line half-compensated current amplitude, thus reducing the effect of the distribution capacitance on the fault component waveform of the normal line current at both ends. In other words, A is

$$A = 0.5U_N * \frac{Y}{2}, \tag{10}$$

where U_{N} is the nominal phase voltage of the system and $Y/2$ is the parallel conductance at both ends of the transmission line π-equivalent circuit.

I_{or}, which is transformed according to the single-loop method, gives the final standard matrix product. There is only one random matrix, i.e., $K = 1$. Remembering the final transformation, the standard matrix product obtained is I_{final}, $I_{\text{final}} \in R^{2m\times 2m}$. I_{final} is the fault identification matrix required in this paper.

(2) Calculation of the Mean Spectral Radius of the Line. In order to eliminate the influence of the eigenvalues of these isolated points on the calculation of the mean spectral radius, these isolated points are first filtered out and then all the eigenvalues are obtained from the fault identification matrix $I\overline{\lambda_i}$, which gives the mean spectral radius r of the line according to the following equation.

$$r = \frac{1}{k}\sum_{i=1}^{k} |\overline{\lambda_i}|, \tag{11}$$

where k is the number of eigenvalues remaining after filtering out the eigenvalues of isolated points.

(3) Fault Line Identification Criteria Based on Random Matrix Spectrum Analysis. The average spectral radius characterizes the difference in waveform between the two terminal current components of the fault, so the average spectral radius r calculated from the real-time data of the two terminal current components of the fault can be compared to a threshold value to identify the faulty line. The threshold value is calculated as follows.

$$r_{sel} = K_{rel}R_s, \tag{12}$$

where K_{rel} is the reliability factor and R_s is the theoretical inner ring radius value.

The two fault detection criteria based on random matrix spectrum analysis are as follows.

(1) Calculate the average spectral radius r_i of line L_i (average spectral radius calculated from the negative and zero sequence currents at both ends of the line r_i^2, r_i^0, the smaller of which is the average spectral radius r of line L_{ii}). If r_i is less than the threshold, then line L_i is determined to be a faulty line. In other words, the fault identification criterion based on random matrix spectrum analysis 1 is

$$\min\left(r_i^2, r_i^0\right) < K_{rel}^{2,0} R_s, \tag{13}$$

$K_{rel}^{2,0}$ is the reliability factor for the average spectral radius calculated from the negative and zero sequence currents and has a value in the range 0.85 to 0.95. The value is set to 0.9.

(2) When a symmetrical fault, tidal current shift, or system oscillation occurs in the system, i the average spectral radius calculated from the positive sequence current fault component r_i^1 is used as the average spectral radius r_i of line L.

$$r_i^1 < K_{rel}^1 R_s, \tag{14}$$

K_{rel}^1 is a reliability factor for the average spectral radius calculated for the positive sequence current fault component. When the system is in symmetry fault, the waveform of the fault component of positive sequence current at both ends of the line is very different, the sequence correlation of the positive sequence fault component is very small, and the average spectral radius is also very small. When the system changes power flow, the waveforms of the positive sequence current fault components at both ends of the line basically coincide. At this point, the average spectral radius does not change much compared to normal operation, but the periodic changes in bus voltage during system oscillations affect the correlation of the sequence of positive sequence current faults at both ends of the line, and the average spectral radius of the line is slightly reduced. In order to avoid the influence of system oscillations on the correlation of the current waveform, the reliability coefficient of the positive sequence current fault component K_{rel}^1 can be set to less than $K_{rel}^{2,0}$, and in this paper K_{rel}^1 set to 0.5.

The fault identification algorithm based on random matrix spectrum analysis essentially uses the time-varying trend characteristics of the current fault component sequence curve to determine whether a fault has occurred on a line.

2.3.2. Wide-Area Backup Protection Algorithm Based on Random Matrix Spectrum Analysis. The steps for wide-area backup security based on spectrum analysis of grid array systems are as follows.

Step 1. Whether each substation satisfies the start-up criteria for the three sequence voltages. If it is satisfied, the three sequence voltages of the buses are sorted and the bus associated with the fault is selected. If $((U_i^2 > K_{rel}^2 U_i^N) \cup (U_i^0 > K_{rel}^0 U_i^N)) = 1$ is satisfied, the fault is an asymmetrical fault and only negative and zero sequence current data are uploaded; if only $(U_i^1 > K_{rel}^1 U_i^N) = 1$ is satisfied, the positive sequence current fault component data are uploaded.

Step 2. Collect the current fault component data L_i on both sides of the bus connection associated with the fault, and then expand the current data at both ends with their historical data to form the matrix I_{final}.

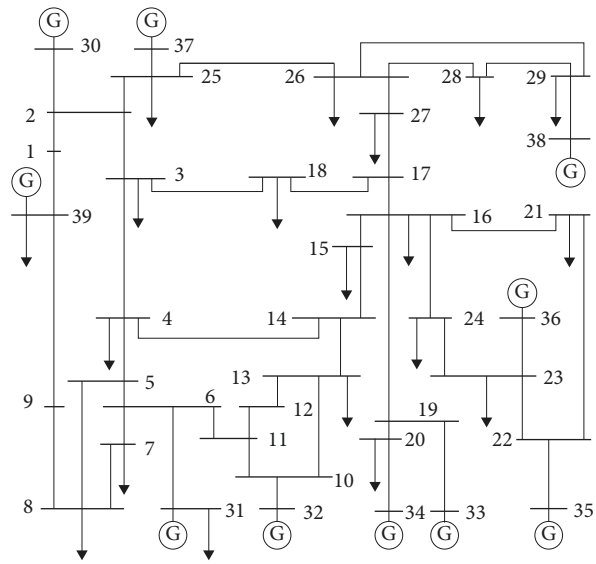

Figure 3: IEEE10 machine 39-node test system.

Step 3. The 2 m eigenvalues of I_{final}; modulate them to obtain $|\lambda_i|$ $(i = 1, \ldots, 2m)$.

Step 4. Calculate the modal value of $|\lambda_i|$, count the number of eigenvalues of the (0, 0.1), (0.1, 0.2) ... (0.9, 1) segments, calculate the probability distribution of $P_{(w,w+0.1)}$ for each segment, and remove the points from $|\lambda_i| > 1$ and $P_{(w,w+0.1)} < 5\%$.

Step 5. After filtering out the nondominated points, obtain $|\overline{\lambda_i}|$, get the average spectral radius r_i, and calculate the theoretical inner ring radius R of the 50×100 high-dimensional matrix I_{final} according to the following equations.

$$R_s = (1 - c)^{B/2} = (1 - 0.5)^{0.5} = 0.707. \tag{15}$$

If the uploaded currents are negative and zero sequence currents, r_i is identified according to criterion 1 of the random matrix spectrum analysis. If the uploaded current is a positive sequence current fault component, the fault line is identified according to criterion 2 of the random matrix spectrum analysis.

3. Experiment

An IEEE standard test system of 10 machines with 39 nodes was built using the electromagnetic transient software PSCAD/EMTDC for simulation and acquisition of relevant experimental data. Transient electromagnetic field refers to electromagnetic field produced by electromagnetic pulse. The research object of this paper includes the law of transient electromagnetic process of pulse or broadband signal in time domain. A diagram of the system structure is shown in Figure 3. The system voltage level is 345 kV, and the frequency is 60 Hz.

Table 1: Test results for line L26_29 under various fault conditions.

Type of fault	Fault location	Transitional resistance/Ω	d	a	Positioning error/percentage	Fault discrimination
AG	0.05	0	1.807	0.057	0.808	L_{26_29}
		100	1.807	0.052	0.246	
		300	1.808	0.052	0.247	
	0.50	0	6.383	0.501	0.209	L_{26_29}
		100	6.365	0.499	0.039	
		300	6.365	0.499	0.039	
	0.95	0	1.151	0.949	0.183	L_{26_29}
		100	1.150	0.948	0.122	
		300	1.150	0.948	0.124	
ABG	0.05	0	1.806	0.056	0.636	L_{26_29}
		100	1.805	0.052	0.249	
		300	1.807	0.052	0.250	
	0.50	0	6.381	0.501	0.139	L_{26_29}
		100	6.364	0.499	0.039	
		300	6.364	0.499	0.040	
	0.95	0	1.150	0.949	0.155	L_{26_29}
		100	1.150	0.948	0.126	
		300	1.149	0.948	0.124	
AB	0.05		1.806	0.057	0.752	L_{26_29}
	0.50		6.383	0.501	0.195	
	0.95		1.150	0.949	0.170	
American Broadcasting Corporation	0.05		1.804	0.051	0.198	L_{26_29}
	0.50		6.403	0.499	0.074	
	0.95		1.149	0.499	0.117	

(1) In the study of algorithms for fault line detection due to normal error sequence components, the sampling frequency was 1.2 kHz. The fault line identification algorithm and fault location were implemented by MATLAB.

(2) In the study of a wide-area random field matrix spectrum for data integrity protection, the sampling frequency was 3 kHz (50 samples per week). The fault identification matrix I was $\text{generated}_{\text{final}}$, and the mean spectrum radius was calculated using MATLAB, where $m = 25$, the data window width is 100 samples ($n = 100$), and the setting threshold is calculated using negative and zero sequence currents: $r_{sel}^{2,0} = 0.9R_x = 0.6364$. The tuning thresholds for the calculation of the fault component of the positive sequence currents are $r_{sel}^{1} = 0.5R_x = 0.3536$.

4. Results and Discussion

Result 1: Fault location simulation based on faulty components.

Result 2: wide-area backup protection simulation based on random matrix spectrum analysis.

To test the effectiveness of the method at different locations and different transition resistances when a fault occurs, line L_{26_29} was selected for testing, with different locations set to 0.25 s and a fault occurring through different transition resistances. The calculated results of **d** and **a for** L_{26_29} after two cycles at the time of the fault are shown in Table 1.

As can be seen from Table 1, the d values do not vary much at the same fault location when the fault line has a metal Earth and high resistance Earth fault, respectively; the d values are also very close when different types of faults occur at the same location. This proves that the calculation results are not influenced by resistance variations and fault types. Fault judgment is only related to the location of fault point, line parameters, and system equivalent impedance. The fault point error is less than 1%, indicating that fault location based on faulty components is better. The table also shows that for phase-to-phase and three-phase short circuits occurring at different locations, the faulted line can be detected by the fault determination quantity d, independent of the fault point location and fault type. For line L_{26_29}, the equivalent impedance on both sides of the line and the ratio of the line impedance is $x = 0.232 < 1$, $y = 0.071 < 1$ and the axis of symmetry is $a_s = 0.42$. For the three fault occurrence points in Table 1, the fault location with $a = 0.5$ is close to the axis of symmetry a_s, which has a larger d value.

As can be seen from Figure 4, phase L_{26_29}, at the onset of the fault, has a steady-state value of approximately 6.3 after two cycles. After the onset of the fault, the d values of the adjacent normal lines L_{25_26} and L_{28_29} increase slightly but are still less than 1. After the transient process is over, the transient process becomes smaller. In addition, it can be seen from the figure that the d corresponding to each line reaches its steady-state value after 0.254 s. The d of the faulty line is much larger than 1, while the d of the adjacent normal line is close to zero. The simulation results show that the implementation of the scheme can accurately detect the faulty lines and that the adjacent normal lines are not misjudged.

(1) In order to verify whether the algorithm can effectively identify fault lines with different ground faults

Table 2: Identification results of the L-line$_{8_9}$ for different fault conditions.

Type of fault	Transitional resistance/Ω	Fault location (%)	r_{8_9}	r_{5_8}	r_{9_39}
AG	0.01	10	0.052	0.840	0.847
		50	0.075	0.841	0.819
		90	0.060	0.858	0.863
	200	10	0.280	0.852	0.846
		50	0.279	0.843	0.845
		90	0.244	0.848	0.848
	300	10	0.358	0.839	0.848
		50	0.353	0.848	0.841
		90	0.322	0.842	0.849
ABG	0.01	10	0.036	0.812	0.851
		50	0.042	0.823	0.844
		90	0.039	0.834	0.832
	200	10	0.268	0.861	0.821
		50	0.270	0.858	0.835
		90	0.277	0.841	0.867
	300	10	0.375	0.838	0.852
		50	0.361	0.858	0.849
		90	0.342	0.857	0.843
AB		10	0.032	0.810	0.842
		50	0.041	0.821	0.830
		90	0.051	0.814	0.831
American Broadcasting Corporation		10	0.035	0.846	0.835
		50	0.042	0.831	0.822
		90	0.017	0.815	0.793

Table 3: Out-of-area test results for faults in the L-line$_{8_9}$ area.

Type of fault	Transitional resistance/Ω	r_{8_9}	Fault discrimination
AG- > BG	0.01 300	0.079 0.359	L_{8_9}
AG- > BCG	0.01 300	0.037 0.352	L_{8_9}
AG- > BC		0.045	L_{8_9}
AG- > CG	0.01 300	0.058 0.384	L_{8_9}

through the transition resistance, line L_{8_9} was selected for testing. L_{8_9} at 0.3 s ground fault, the fault line, and its adjacent lines of the average spectrum radius is shown in Table 2.

As can be seen from Table 2, the average spectral radius does not change significantly with the location of the fault point for the same fault condition. The algorithm can correctly identify faulty lines under different fault conditions with different transition resistances at different locations to Earth. At 345 kV, the algorithm correctly identifies the fault line when the transition resistance reaches 300 Ω.

(2) To verify the action characteristics of the fault protection in the out-of-zone transition zone, a 0.2 s A-phase metallic Earth fault is set on the protective outlet of bus 5 of line L_{5_8} and the protective outlet of bus 25 of L_{25_26}. After 0.1 s transition to the line L of 10% bus 8 and $L_{8\_926\_29}$ of 10% bus 26 ground fault, the average spectral radius after 2 cycles of the fault is shown in Table 3. The average spectral radius of the line L_{8_9} out-of-zone transition zone fault changes is shown in Figure 5.

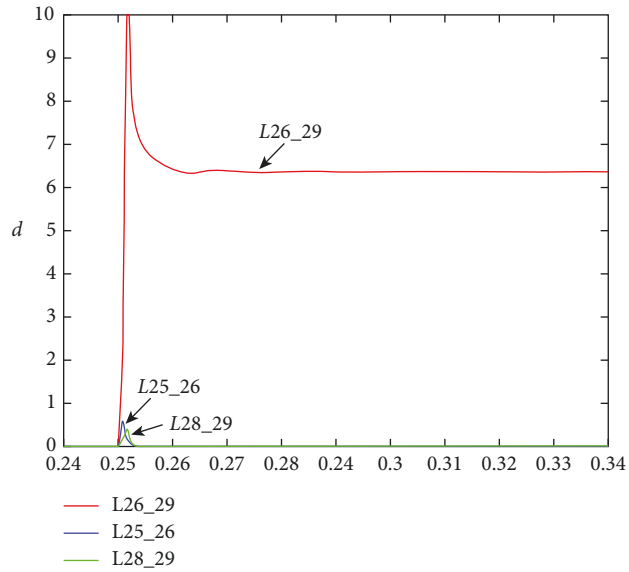

Figure 4: Plot of the change in d value of L_{26_29}, which is 50% at 0.25 s.

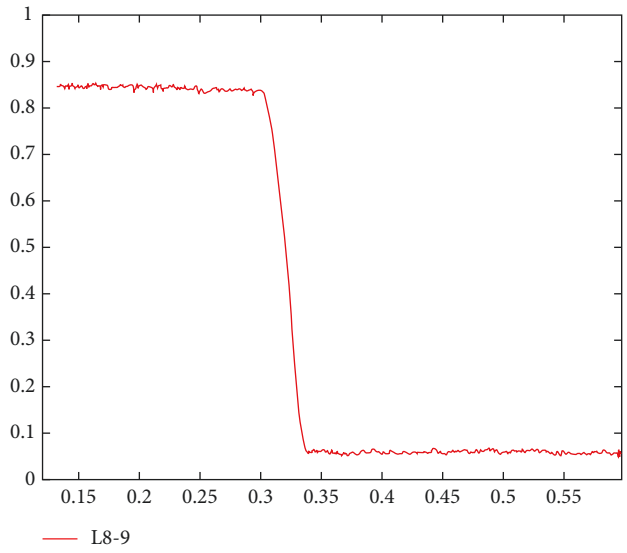

Figure 5: Variation in the mean spectral radius of L-lines in the out-of-zone fault zone 8_9.

As can be seen from Table 3, an out-of-area fault is transferred to an in-area fault. Whether the fault is transferred to a metallic Earth fault in the zone or to a high resistance Earth fault in the zone, the average spectral radius of the two cycles after the fault occurs is less than the threshold value of 0.636, allowing accurate identification of the faulty line. As can be seen in Figure 5, the adjacent line is faulted at 0.2 s at the protection outlet of bus 5, and the average spectral radius value of the line L_{8_9} remains stable. When the fault is transferred from the outside to line L8_9, the average spectral radius value of line L_{8_9} drops rapidly, is below the given threshold, and is judged to be a faulty line.

5. Summary

Based on existing research on wide-area backup protection, this paper proposes a fault line identification current error element calculation method using line terminals and a defense algorithm based on wide-area backup random field analysis. The simulation results show that the results of the proposed method can accurately identify faulty lines under various fault conditions. However, there are still some shortcomings in this study that require further research.

(1) The experimental environment is ideal, while there are many influencing factors in the actual scenario. For example, the capacitance to ground of long distance transmission lines of extra high voltage may affect the fault location accuracy of the algorithm. This needs to be considered in subsequent studies.

(2) The effect of measurement noise on fault location accuracy has not been investigated. The effect of this factor on the performance of the algorithm needs to be further explored.

Research on key technologies of wide-area backup protection of smart DC power grid based on fault identification is also of great significance to promote the development of wide-area backup protection technology of smart DC power grid.

Data Availability

No data were used to support this study.

Conflicts of Interest

The authors declare that there are no conflicts of interest regarding the publication of this article.

Acknowledgments

This work was supported by the Central Guidance on Local Science and Technology Development Fund of Tibet Autonomous (Grant no. XZ202201YD0022C).

References

[1] C. Zhang and H. Wang, "Analysis of the current situation of power system and automation and improvement measures," *Science and Technology Innovation*, no. 22, p. 120, 2014.

[2] F. Wang, F. J. Shen, and J. Li, "Design of load dumping risk monitoring function for large-scale urban power grid security and stability control devices," *Automation of Electric Power Systems*, vol. 40, no. 20, pp. 161–167, 2016.

[3] F. Zeng, F. Sun, and T. Li, "Analysis of the "9-28" blackout in Australia and its implications for China," *Automation of Electric Power Systems*, vol. 41, no. 13, pp. 1–6, 2017.

[4] D. Wu, "Analysis of rapid excision and isolation of distribution line faults," *Electronics Test*, vol. 403, no. 22, pp. 76-77+136, 2018.

[5] G. Huang, "Simulation of relay safety protection for low-voltage distribution networks in power supply systems," *Computer Simulation*, vol. 35, no. 2, pp. 63–66, 2018.

[6] B. Ingelsson, P. O. Lindstrom, D. Karlsson, G. Runvik, and J. O Sjodin, "Wide-area protection against voltage collapse," *IEEE Computer Applications in Power*, vol. 10, no. 4, pp. 30–35, 1997.

[7] Y. Serizawa, M. Myoujin, K. Kitamura et al., "Wide-area current differential backup protection employing broadband communications and time transfer systems," *IEEE Transactions on Power Delivery*, vol. 13, no. 4, pp. 1046–1052, 1998.

[8] B. Mallikarjuna, P. V. V. Varma, S. D. Samir, M. J. B. Reddy, and D. K. Mohanta, "An adaptive supervised wide-area backup protection scheme for transmission lines protection," *Protection and Control of Modern Power Systems*, vol. 2, no. 1, pp. 22–25, 2017.

[9] S. S. Mirhosseini and M. Akhbari, "Wide area backup protection algorithm for transmission lines based on fault component complex power," *International Journal of Electrical Power & Energy Systems*, vol. 83, pp. 1–6, 2016.

[10] H. Jia, K. Xue, and J. Ma, "Improved ant colony algorithm for multipath routing of wide path protection communication," *Automation of Electric Power Systems*, vol. 40, no. 22, pp. 22–26, 2016.

[11] F. Shan, Z. Ma, and J. Gao, "A wide-area backup protection algorithm based on information fusion," *Science and Technology Innovation*, no. 7, p. 92, 2016.
[12] J. Liu, K. Zhang, and Q. Tian, "Wide-area standby protection algorithm based on sequence current gray correlation analysis and multi-information fusion," *Power System Protection and Control*, vol. 46, no. 19, pp. 25–31, 2018.
[13] G. Song, J. Jiang, and W. Li, "Highly fault-tolerant wide-area backup protection algorithm based on," *IED*, vol. 12, no. 12, pp. 11–17, 2017.
[14] J. H. He, Z. Q. Wang, and H. H. Zhang, "A wide-area backup protection partitioning method based on graph theory and fuzzy evaluation," *Power Automation Equipment*, no. 2, pp. 75–82, 2017.
[15] X. Y. Tong, W. C. Lian, and Y. F. Teng, "Wide-area standby protection using differential active power immunity under finite PMU," *Proceedings of the CSEE*, vol. 38, no. 8, pp. 2335–2347, 2018.
[16] W. Cunxiang and X. Chang, "Wide-area standby protection scheme for urban rail transit power supply system," *Highways*, no. 07, pp. 354–358, 2017.
[17] H. B. Wang, R. Z. Wang, and X. Y. Tong, "Wide-area standby protection fault line identification algorithm based on multipoint PMU voltage estimation," *Electrical Applications*, no. 20, pp. 50–55, 2016.
[18] H. Tang, "Multi-information fusion wide-area backup protection based on ant colony algorithm," *Communications Power Technology*, vol. 34, no. 2, pp. 44-45, 2017.
[19] T. Wang, "Longitudinal tear image detection and identification method of longitudinal tear in mining conveyor belt," *Modern Business & Industry*, no. 24, pp. 202–204, 2018.
[20] W. Wang, Y. Li, and L. Z. Ge, "Identification of series DC arc faults based on sliding discrete Fourier transform," *Transactions of China Electrotechnical Society*, no. 19, pp. 122–128, 2017.
[21] D. Zhu, J. Shen, and Y. Huang, "Industrial fault identification based on active learning and weighted support vector machines," *Journal of Zhejiang University*, vol. 51, no. 4, pp. 697–705, 2017.
[22] X. Jia, J. L. Zhang, and X. B. Wen, "Double-supervised signal deep learning for infrared fault identification of electrical equipment," *Infrared and Laser Engineering*, vol. 47, no. 285, pp. 32–38, 2018.
[23] W. Ma, M. Lei, and B Liu, "Fault identification of power machine bearings of packaging machinery based on ICS-LSSVM," *Packaging Engineering*, vol. 39, no. 11, pp. 176–181, 2018.
[24] G. Chen, "Analysis of fault identification and treatment measures for transmission and distribution lines," *Indonesian Journal of Electrical Engineering and Computer Science*, vol. 8, no. 1, pp. 199–205, 2017.
[25] S. Li and L. Cai, "Wind turbine blade crack identification based on aerodynamic signal analysis," *Journal of Vibration and Shock*, no. 19, pp. 235–239, 2017.